Available online at www.sciencedirect.com

jmr&t Journal of Materials Research and Technology

www.jmrt.com.br

Original Article

Exfoliation corrosion susceptibility in the zones of friction stir welded AA2098-T351

Mariana X. Milagre[a,*], Uyime Donatus[a], Caruline S.C. Machado[a], João Victor S. Araujo[a], Raphael O. Ferreira[b], Rejane Maria P. Silva[a], Renato A. Antunes[c], Isolda Costa[a]

[a] Instituto de Pesquisas Energéticas e Nucleares – IPEN/CNEN – Av. Prof. Lineu Prestes, 2242, São Paulo, Brazil
[b] Escola Politécnica da Universidade de São Paulo, PMR/USP, Av. Prof. Mello Moraes, 2463, São Paulo, SP, Brazil
[c] Universidade Federal do ABC, Centro de Engenharia, Modelagem e Ciências Sociais Aplicadas. Av. dos Estados 5001, Santo André, Brazil

ARTICLE INFO

Article history:
Received 26 December 2018
Accepted 24 September 2019
Available online 16 October 2019

Keywords:
Exfoliation
Aluminum alloys
Friction stir welding

ABSTRACT

In the present study, the exfoliation susceptibility of the weld zones in friction stir welded AA2098-T351 was compared with that of the base metal (BM) according to ASTM G34 standard practice. Friction stir welding (FSW) had a significant effect on the microstructure of the Al alloy tested and the susceptibility to exfoliation was strongly affected by the microstructure. Different features of corrosion attack and exfoliation susceptibility were observed when the zones affected by FSW were tested isolated or coupled. Also, the near-surface deformed layer had an important effect on the Al alloy susceptibility to exfoliation. These are the main findings of this work. The corrosion features were correlated with the microstructural modifications related to the welding process and with the electrochemical response. The T1 phase morphology, distribution and size were critical for exfoliation susceptibility. The stir zone (SZ) was the zone most resistant to exfoliation. However, resistance to exfoliation varied with the temperatures reached in the heat affected zones (HAZs). The HAZ exposed to the lowest temperatures during welding, HAZ (LT), was the most susceptible to exfoliation, whereas the HAZ exposed to the highest temperatures, HAZ (HT), presented high resistance to exfoliation, similarly to the SZ. The ASTM-G34 practice was an effective and useful method in identifying the different exfoliation resistances of the BM and the various zones affected by FSW. The results of this practice were supported by electrochemical impedance spectroscopy (EIS) tests.

1. Introduction

The Al-Cu-Li alloys are highly susceptible to localized corrosion, such as pitting, intergranular corrosion (IGC) and exfoliation [1,2]. This susceptibility is closely related to the microstructural features of this kind of alloys.

Exfoliation is a kind of IGC where the volume of the corrosion products formed at the grain boundaries (GBs) is sufficient to cause blisters. The continuity of this process increases the pressure at this region until the point where the stress limit of the alloy is reached and the blisters are opened. For this purpose, the literature presents some microstructural charac-

* Corresponding author.
E-mail: marianamilagre@yahoo.com.br (M.X. Milagre).
https://doi.org/10.1016/j.jmrt.2019.09.066

teristics that can increase the susceptibility of Al-alloys to this type of corrosion [3].

Robinson and Jackson [4] showed how the grain structure influences exfoliation and stress corrosion cracking in high strength Al-alloys. Also, Kelly and Robinson [5] reported on the influence of heat treatment and grain morphology on exfoliation of Al-Li alloys. Chen et al. [6] also described the effects of heat treatment on exfoliation susceptibility. The relationship between alloy composition, microstructure and exfoliation corrosion was also reported by Marlaud et al. [7] for an Al–Zn–Mg–Cu alloy.

In general, exfoliation susceptibility is influenced by a combination of grain shape and morphology and distribution of the phases. The role of the T1 phase (Al_2CuLi) on the corrosion behavior of Al-Cu-Li alloys has been largely reported [8–11]. Li et al. [12] observed that exfoliation susceptibility increases with the increase in T1 phase content and equilibrium size at the GBs.

Yue et al. [13] proposed that the formation of galvanic couples between the T1 phase or θ' (Al_2Cu) phases and precipitate free zones (PFZ) is the main cause of IGC and, exfoliation susceptibility in the AA2195 alloy. Liang et al. [14] reported that as the T1 phase coarsens and wide PFZs are formed, the susceptibility to IGC and exfoliation increases.

Friction stir welding (FSW) processes modify the microstructural features of the Al-Cu-Li alloys [15–18] and, as a consequence, the corrosion susceptibility of the different regions along the weldment [19–22]. FSW consists in joining two parts of materials without melting. However, the heat and deformation generated by the process promote microstructural modifications which are sufficient to affect the corrosion susceptibility across the weld. Since each welding process is considered unique as the welding parameters can influence corrosion susceptibility [21,23], it is important to investigate the susceptibility to corrosion of the different zones in welded alloys by FSW.

The AA2098 is a representative alloy of the advanced third generation Al-Cu-Li alloys developed for applications in the aerospace industry in search of potential replacements for the conventional Al-Cu alloys. This alloy was the precursor of the AA2198 alloy whose corrosion behavior has been reported in the literature [1,2,8,24]. However, studies on the corrosion susceptibility of the AA2098 are very scarce [25] and no information was found on the resistance of this alloy to exfoliation. Moreover, works on the effects of FSW on exfoliation resistance of Al-Cu-Li alloys are rare in the literature [2,26]. Based on the fact that each welding process is unique due to the effects of welding parameters and tool geometry on the microstructure of Al-Cu-Li alloys, the present study contributes to the field of knowledge on corrosion resistance of this kind of alloys by investigating the exfoliation resistance of the AA2098-T351, by electrochemical techniques and surface observation.

The use of electrochemical techniques in the study of exfoliation susceptibility of aluminum alloys has been previously reported [6,27–30], but none of these works studied Al-Cu-Li alloys. Keddam et al. [27] showed how electrochemical impedance spectroscopy (EIS) could provide useful information about the trends in the mechanism of the exfoliation process in conventional Al-alloys. In this work, the exfoliation susceptibility of the weld zones of the AA2098-T351 alloy resulting from FSW was analysed and the results were compared with that of the base metal (BM). The effects of surface preparation on the exfoliation susceptibility were also analyzed. The evaluation was performed according to ASTM-G34 standard. The results were correlated with the microstructural features, surface composition in different conditions (as received and polished) along the weldment and with the electrochemical response of the alloy.

2. Material

Friction stir welded 3 mm thick plates of the AA2098-T351 alloy were used in this work. The alloy is composed of 3.4 wt% Cu, 1 wt% Li, 0.3 wt% Mg, 0.3%wt Ag, 0.4 wt% Zr, 0.04 wt% Fe, 0.05 wt% Si, 0.02 wt% Zn, and 0.003 wt% Mn.

2.1. *Friction stir welding (FSW) process*

FSW process was performed using an H13 steel tool with a shoulder of 16 mm diameter and an adjustable pin in accordance with the plate thickness. Transverse speed was 300 mm/min and the rotation speed was 700 rpm in the counter-clockwise direction. Thus, the retreating side of the weldment was on the left and the advancing side was on the right, Fig. 1(a). The load used was in the range of 8–15 kN. Thermal profile simulation was obtained using the finite element COMSOL v5.2 software. Thermocouples measurements were carried out as input data. They were positioned under the plate, at distances of 6, 9 and 12 mm from the center of the welding joint, Fig. 1(b). More details on the thermal simulation are provided in our previous work [15].

2.2. *Microstructural characterization*

The surface was prepared by metallographic techniques. Mechanical polishing was carried out using silica carbide abrasives (#320, 550, 800, 1200, 4000) and diamond suspensions of 3 and 1 μm. An etching solution composed of 25% HNO_3 and 3% HF in deionized H_2O was used to reveal microstructural features. Electrolytic etching was performed in a solution composed of 20 vol% nitric acid in methanol at 25 V and −30 °C prior to the acquisition of transmission electron microscopy (TEM) images. The TEM samples were prepared using a TenuPol equipment. Imaging was carried out using a JEOL 2100 microscope. Optical and scanning electron microscopy (SEM) images were acquired using a Leica model DMLM optical microscope and a Hitachi TM 3000 scanning electron microscope with an incident beam of 15 keV. Microhardness profile was obtained using a Knoop/Vickers Tukon 1202 Wilson Hardness tester. Microhardness measurements were carried out on the polished surface of the welded sample in steps of 0.2 mm using a load of 200 gf for 10 s.

2.3. *X-ray photoelectron spectroscopy (XPS)*

The chemical composition of the sample surfaces was analyzed by X-ray photoelectron spectroscopy (XPS) using a ThermoFisher Scientific spectrometer, model K-alpha$^+$, oper-

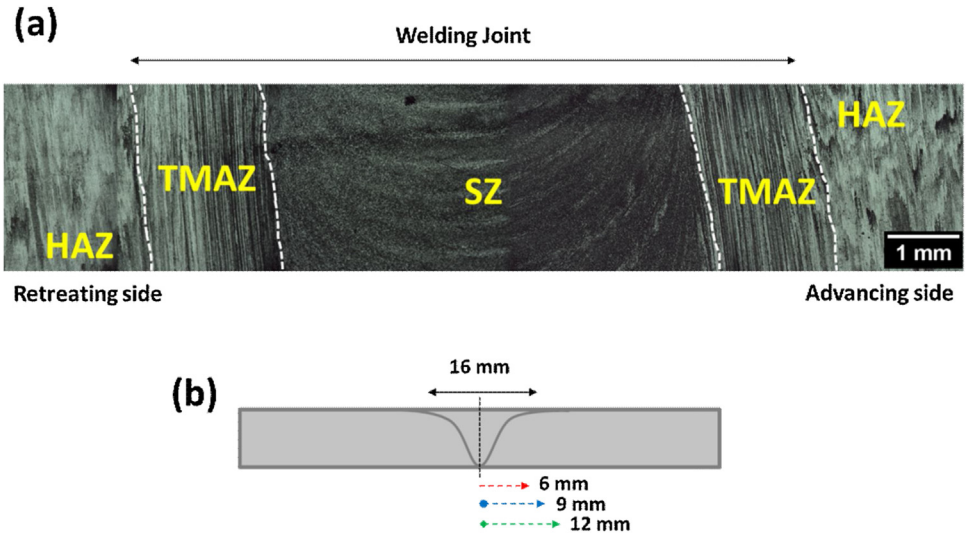

Fig. 1 – (a) Optical microscopy of the friction stir weld showing the welding zones; (b) schematic diagram showing the position of the thermocouples during the welding process.

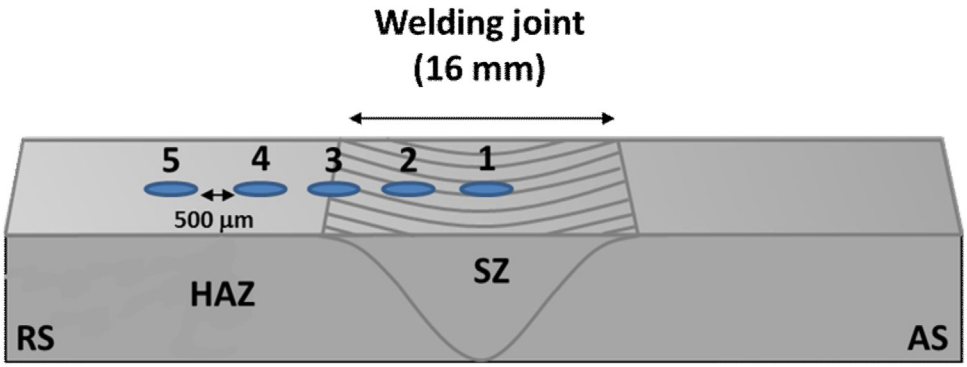

Fig. 2 – Schematic diagram showing the points from where XPS measurements were taken.

ating with a monochromatic Al K-α X-ray source. The spot size was 400 μm, and the analysis chamber pressure was 10^{-7} Pa. Survey XPS spectra of the welded samples at different zones and, in the different conditions of preparation (as received, polished) were obtained, as provided in Fig. 2.

2.4. *Exfoliation susceptibility*

Exfoliation susceptibility test was performed according to ASTM G34 practice. Prior to immersion, the surfaces of the specimens were cleaned with isopropyl alcohol in an ultrasonic bath for 10 min. After surface preparation, the samples were immersed for 48 h in the test solution composed of 234 g of NaCl, 50 g of KNO_3, 6.3 mL of HNO_3 (70 wt.%) and deionized water until 1 L. The pH of the test solution was 0.4. After 48 h, the samples were removed from the constant immersion exfoliation corrosion (EXCO) solution, rinsed with deionized water and dried at room temperature.

2.5. *Electrochemical impedance spectroscopy (EIS)*

Electrochemical impedance spectroscopy (EIS) tests were carried out using an AUTOLAB PGSTAT potentiostat controlled by NOVA 1.11 software. The tests were performed at room temperature using a three electrode-cell setup with $Ag/AgCl_{KCl(sat)}$ as a reference electrode and a platinum wire as the counter electrode. The exposed surface of the working electrode was 25 mm^2. The welding zones analyzed were identified according to microstructural features and corrosion behavior, as described in the next sections. The welding zones were individually masked using bee wax. Unwelded base material (BM) samples were used for comparison. For the electrolytes, the standard solutions for the EXCO test were used and each welding zone was exposed for 1 h to the electrolyte before the EIS data acquisition. The EIS data were obtained potentiostatically at the OCP in the frequency range of 100 kHz to 0.1 Hz with a 10 mV amplitude signal and an acquisition rate of 10 points per decade. EIS tests were performed on as-received surfaces and surfaces mechanically polished to #4000 SiC paper surface finish.

3. Results and discussion

Surface and microstructural characterization

In order to evaluate whether the welding process affected the external layer, XPS measurements were carried out on

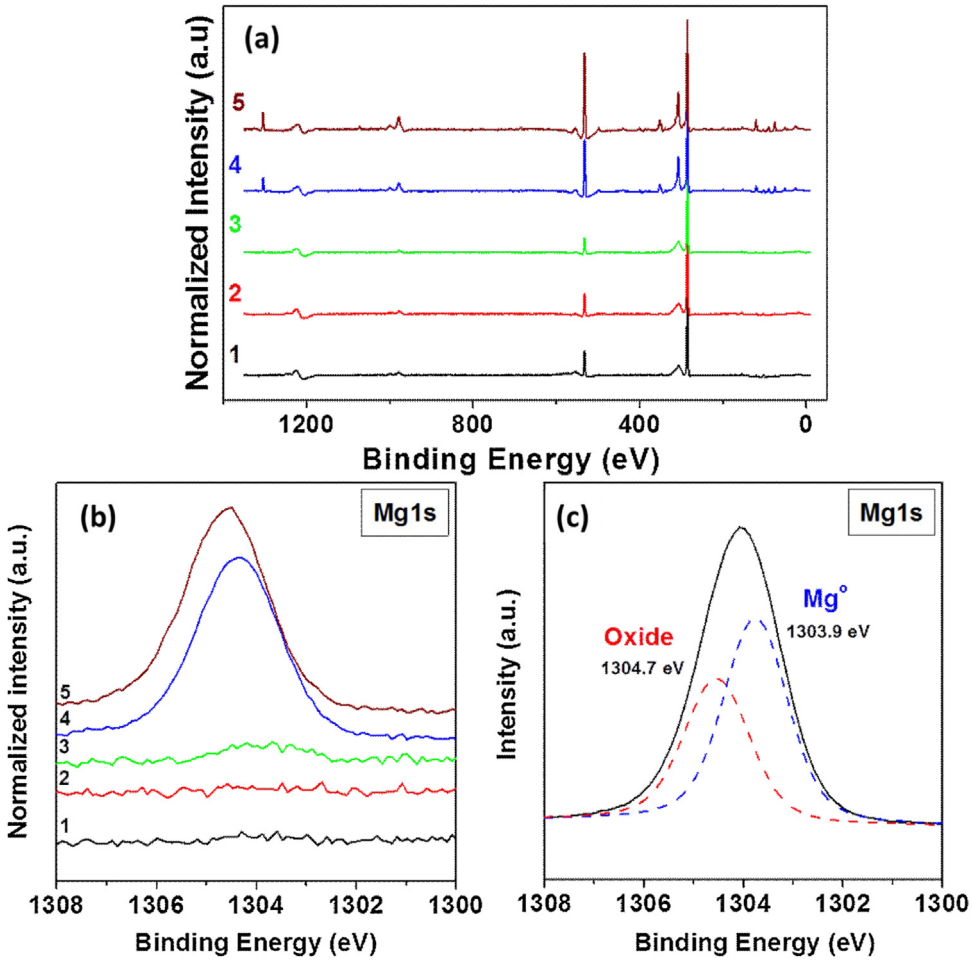

Fig. 3 – Variation of surface composition of the as-received AA2098-T351 welded by FSW. (a) Survey spectrum using AlKα radiation; (b) high-resolution spectra for Mg at different zones of the Al alloy welded by FSW; (c) Mgs1 high-resolution spectra deconvolution.

the different weld zones. Elements such as Al, O, Mg, and Cu were observed in the external layer, Fig. 3a. The main chemical composition variation in the external layer comparative to the bulk alloy was related to the Mg content. Fig. 3b shows the presence of Mg-enriched bands in the outer layer of the studied alloy. This has been related to the activity of this type of material [24,31,32,33]. The spectra corresponding to the region close to the welding joint in Fig. 3b, points 1–3, show reduction in Mg content. This was due to the removal of the external layer by the welding process. However, analysis carried out on a polished welded sample also showed variations in the composition of the outer layer of the surface, Fig. 4a. A slight reduction in Mg content was observed in addition to Cu content increase in the welding joint region. Binding energies between 933.6 and 953.2 eV, Fig. 4b, indicate that the Cu signal comes from the substrate and the Cu enriched intermetallic particles in the alloy [25,34]. The influence of the FSW process on the microstructure of the AA2098-T351 was reported in a previous work [15]. The temperatures reached during the FSW process are sufficient to promote T1 phase (Al_2CuLi) dissolution and Cu diffusion to the matrix Moreover, the tool movement during the welding process promotes breakage of micrometric particles in the tool domain [35] increasing the area related to micrometric particles in the welding joint region. Consequently, the Cu signal in the welding joint increased. According to the literature [36], the peak with binding energy around 1304.7 eV is related to Mg oxides, Fig. 3c. Besides, a peak with binding energy around 1303.9 eV was related to metallic Mg [37]. However, when the outer layer is removed due to welding or polishing processes, only the Mg signal in solid solution is observed, Fig. 4b.

Furthermore, the temperatures reached at some areas of the alloy during the welding process changed the T1 phase content along the weldment. The T1 phase is the main strengthening phase in Al-Cu-Li alloys. It precipitates preferentially at dislocations and subgrain boundaries [38] at temperatures between 137 and 260 °C. This phase has a hexagonal crystal structure with an orientation of $(0001)_{T1}$ // $\{111\}_{Al}$ and $<10\ \bar{1}\ 0>_{T1}$ // $<110>_{Al}$ and a platelet morphology [39].

The highest content of T1 phase is found in the BM, Fig. 5a, whereas its density is significantly lower in the HAZ, Fig. 5b. In this last zone, the T1 phase is coarser and shorter than in the BM. Besides, wider PFZs are observed in the HAZ relative to the BM. In the SZ, Fig. 5c, T1 is rarer, shorter and coarser compared

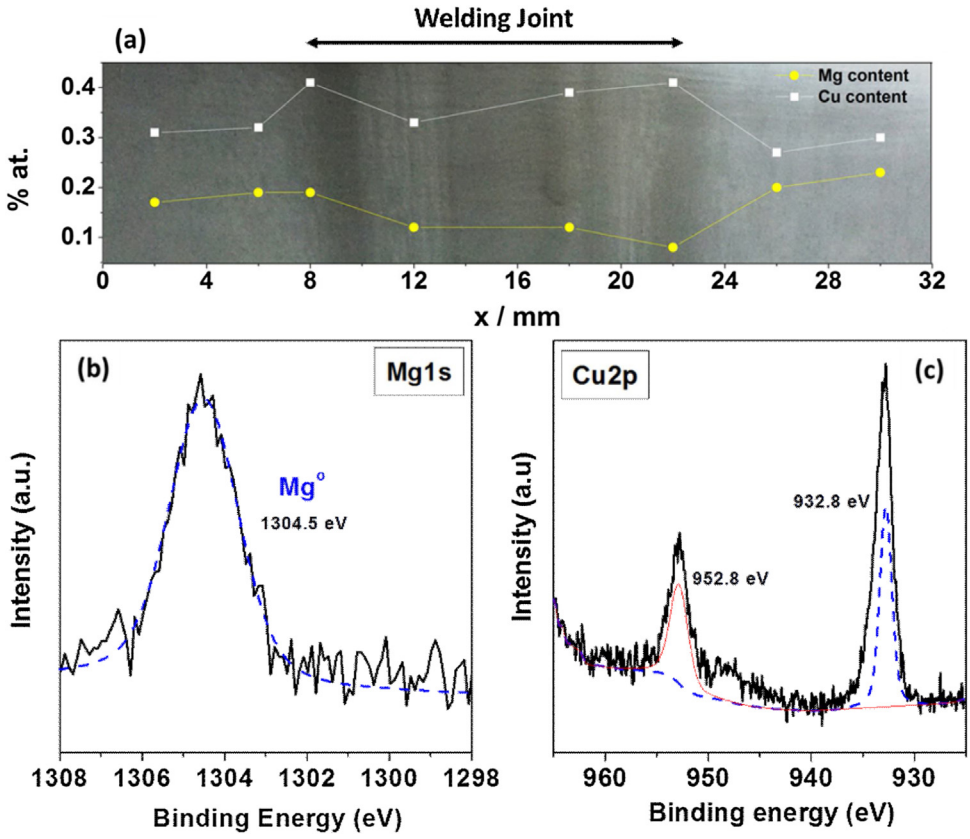

Fig. 4 – Cu and Mg atomic content obtained by XPS analysis along a polished surface of the AA2098-T351 alloy welded by FSW.

to the BM. In the BM, the T1 phase is finely dispersed at the GBs and inside the grains. This is due to the stretching step prior to aging, that is represented by the "51″ nomenclature. Stretching results in stress relief but also increases the dislocation density, which favors nucleation and precipitation of T1 phase [40]. The thermal cycles of the welding process lead to partial or total T1 phase dissolution. In the HAZ, the temperatures reached during FSW are not sufficient for total dissolution of T1 phase, and, consequently, some precipitates are coarsened and others nucleate, being of smaller sizes. According to Chen and Bhat [38], the T1 phase has a strong tendency to nucleate at subgrain boundaries. Since its growth is fast, this phase is usually thicker and shorter than the same type of precipitate that grows in the matrix, as observed in Fig. 5b. Finally, in the SZ, dynamic recrystallization process occurs leading to reduced dislocation density and T1 phase dissolution. Consequently, the T1 plates are thin, since the fast dissipation effect reduces the time available for nucleation and growth of strengthening phases.

3.1. *Exfoliation Susceptibility*

Fig. 6 shows one of the AA2098-T351 samples during exposure to the EXCO test for environment assessment. Very high activities were observed in the BM with the formation of voluminous amounts of hydrogen bubbles. However, in the welded sample, lower reactivity and, consequently, higher exfoliation resistance compared to the BM was found. Fig. 7 shows the cross-section of the BM after exposure to EXCO test. It can be seen that this region presents high susceptibility to exfoliation. In this zone, intragranular corrosion was the preferential type of attack with two types of intragranular attack observed. The first type is characterized by the total consumption of the grain (grain A), whereas the second one is only associated with some particular grains, that is, orientated attack aligned in the grain elongation direction (grain B). There are several factors that affect the morphology of attack, such as grain size and grain orientation, in relation to the electrolyte [10,41,42]. According to Guérin et al. [41], the most relevant parameter for intragranular corrosion in Al alloys is their internal disorder. Thus, grains with large number of defects are the most susceptible to corrosion. The authors observed that the grains orientated according to (111) plane in relation to the electrolyte are completely attacked (grain A). This occurs because the (111) planes are parallel to the deformation direction. Therefore, the dislocation and T1 phase densities are higher and evenly distributed in these grains and their GBs, Fig. 4a. Consequently, potential differences between grains and GBs were not significant, resulting in intragranular attack. The attack in bands parallel to $\{111\}_{Al}$ direction indicates that corrosion propagation depends on grain orientation. This type of attack is known as crystallographic attack and has been reported in the literature [1,42,43]. The attack in preferential directions (grain B) is related to the stretching step prior to nat-

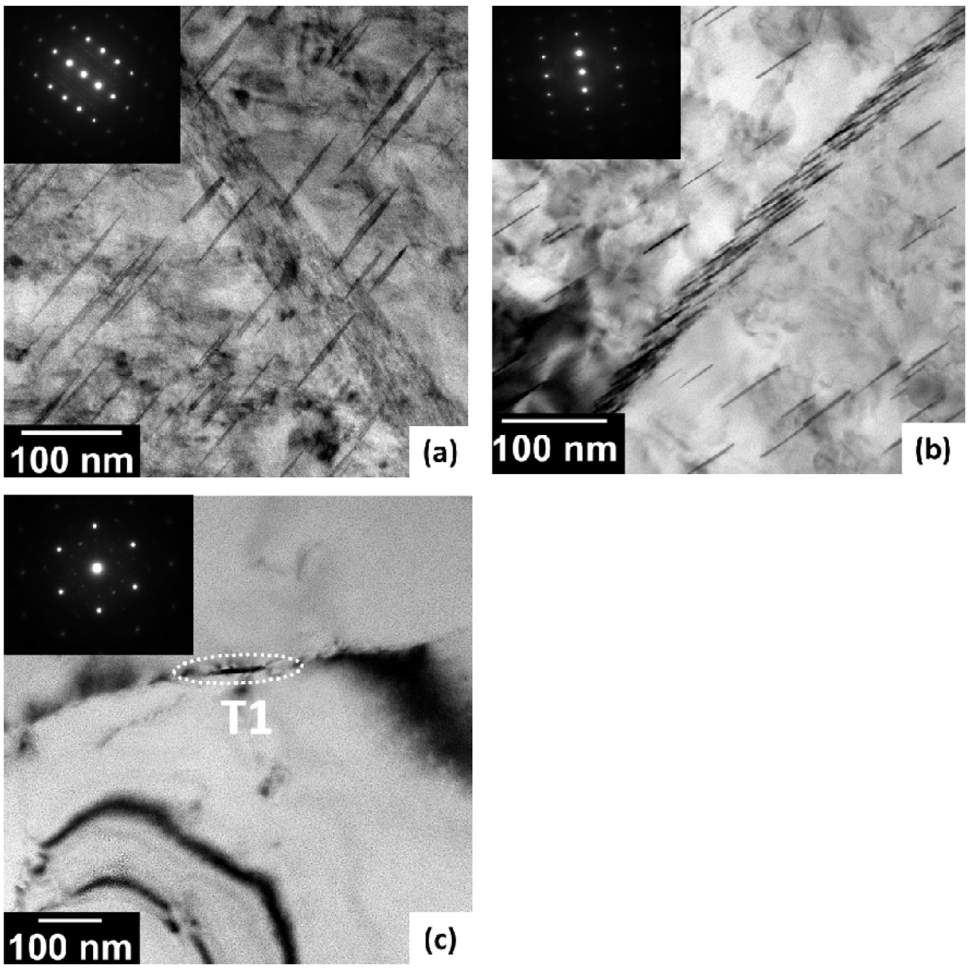

Fig. 5 – TEM bright-field image of the grain boundary showing variations in T1 phase density, morphology and size according to the different zones; (a) BM; (b) HAZ; (c) SZ.

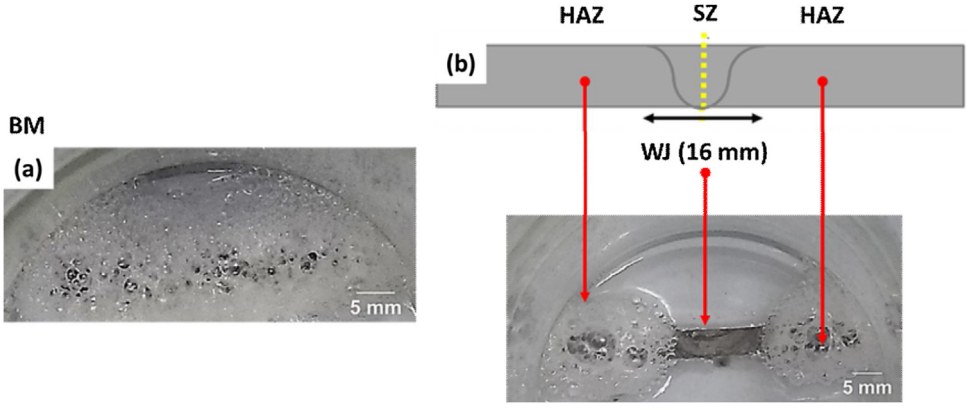

Fig. 6 – Optical images of the (a) unwelded alloy (BM) and (b) welded samples of the AA2098-T351 during EXCO test.

ural aging. During this process, slip bands originate as a result of heterogenous plastic stresses due to the high stacking fault energy of Al alloys [44], resulting in increased T1 phase density in the bands [45].

Fig. 8 shows the susceptibility of the welded sample to exfoliation. A relationship between exfoliation susceptibility and T1 phase concentration and morphology is indicated. The HAZ was divided into two regions of different resistances to exfoliation. The areas in the HAZ corresponding to a high decrease in hardness are the ones exposed to the highest temperatures during welding, HAZ (HT). The temperatures reached in these zones were in the range of 300–380 °C, in the advancing side,

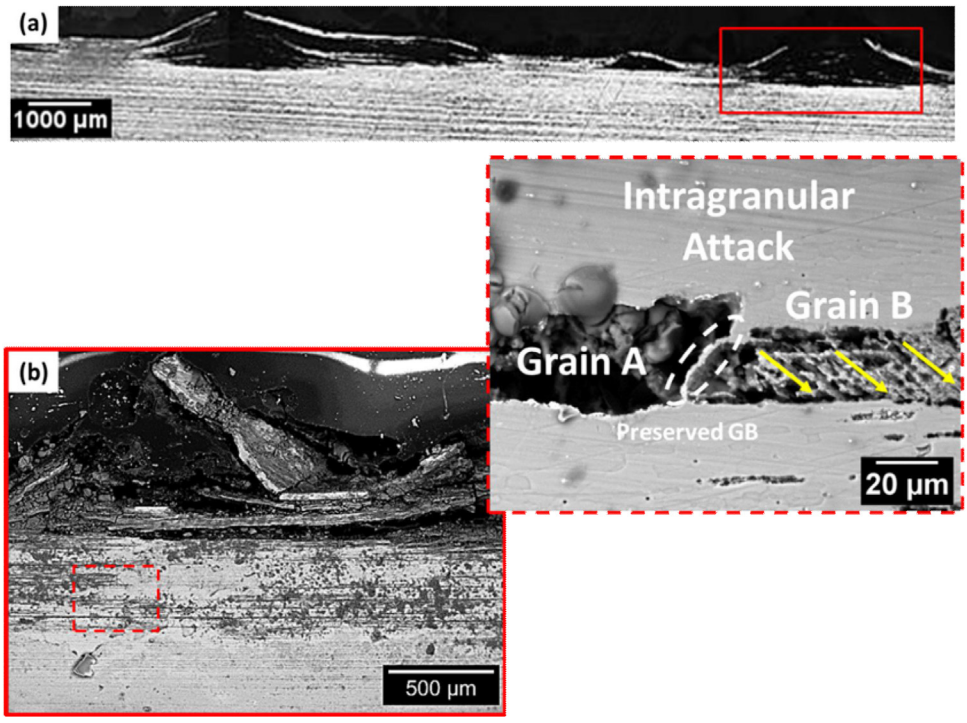

Fig. 7 – Cross-sectional views of the AA2098-T351 alloy after 48 h exposure to EXCO solution showing different susceptibilities to exfoliation.

and between 240 to 320 °C, in the retreating side. This zone showed high resistance to exfoliation. On the other hand, the regions of the HAZ exposed to the lowest temperatures, HAZ (LT), presented the highest activities in the EXCO solution. The microhardness in this zone is lower in relation to the BM and the temperatures reached were less than 300 °C, in the advancing side, and 240 °C, in the retreating side. These results confirm the direct effect of T1 phase on the exfoliation susceptibility of the AA2098-T351. It is important to highlight that in the HAZ (LT), intragranular corrosion predominated, although IGC was also seen. This behavior is related to the T1 phase morphology which was coarser and shorter in this region. Also, PFZs were associated with the HAZ (LT).

The morphology of attack propagation also changed according to the welding zone, Fig. 9–11. In the HAZ (LT), Fig. 9a, similar exfoliation features to those of the BM were found. Grains with higher T1 phase content were anodic in relation to those with lower amounts of T1 phase. Moreover, Cu and Ag redeposition was found on the cathodic sites surrounding the anodic areas showing high susceptiblility to exfoliation in the HAZ (LT), Fig. 9b. The Cu enters the test solution by the detachment of Cu-rich particles from the attacked areas. In the solution, the potential of these particles increased which leads to Cu dissolution, and this is followed by Cu redeposition at the cathodic areas surrounding the anodic ones [46,47]. The Ag is also a noble element in relation to Al and is added to the Al-Cu-Li alloys to enhance T1 phase precipitation [48]. The identification of these elements around the anodic sites shows the effect of the T1 phase on the corrosion behavior of the AA2098-T351. Intergranular corrosion was also observed in the HAZ (LT). The smaller and coarsened T1 phase, in addition to the wider PFZ of the HAZ (LT) in relation to the BM, are the reasons for this type of attack propagation. The HAZ exposed to high temperatures (HT), Fig. 10, and the welding joint (TMAZ + SZ), Fig. 11, when coupled to the other zones, were cathodically protected. In the HAZ (HT), only a few and isolated grains presented intergranular attack, either in the retreating (Fig. 10a) or advancing sides (Fig. 10b). In the welding joint, no attack was observed, Fig. 11. These behaviors are related to the galvanic coupling established between regions of high density of T1 phase (BM and HAZ (LT)) acting as anodes, and regions of low T1 phase density (HAZ (HT), TMAZ and SZ), acting as cathodes. In the welding joint, other factors favor the cathodic behavior of this region, such as, increased Cu and decreased Mg contents, besides the larger proportion of area corresponding to Al-Cu-Fe particles, which are efficient cathodes [49], at the exposed surface.

EIS analysis was carried out to understand the exfoliation mechanism in the AA2098-T351. The polished samples were related to lower impedances indicating lower resistance to exfoliation than the unpolished (as-received) ones, Fig. 12a-b. The low impedances and the presence of only one-time constant showed that both types of surface, polished or unpolished were highly active in the EXCO solution. The results did not indicate the presence of a surface oxide film, which is explained by the high aggressiveness of the solution to the surface. Fig. 12c shows the unpolished surface after exposure to the EXCO solution for the EIS test. It can be seen that the attack is localized while the majority of the surface is preserved. This result can be related to the presence of Mg oxide on the

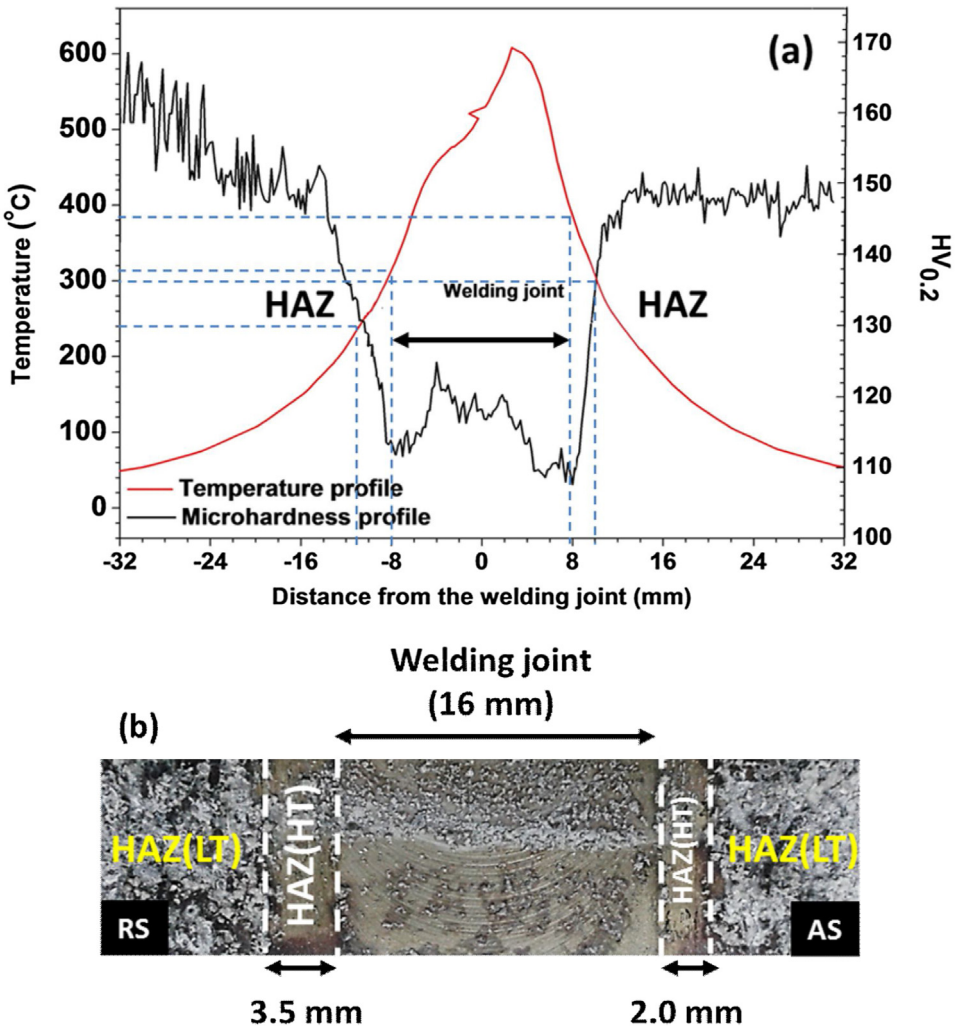

Fig. 8 – Correlation between microhardness, temperature and exfoliation susceptibility; (a) microhardness and temperature profile during the welding process. The welding zones which reached the highest temperatures are the regions with the lowest microhardness values. (b) Macroscopic image of the AA2098-T351 welded by FSW after 48 h immersion in EXCO solution. The welding zones with the lowest microhardness values are the regions of highest resistance to exfoliation. HAZ (LT) = heat affected zone where comparatively lower temperatures were reached; HAZ (HT) = heat affected zone where comparatively higher temperatures were reached, in the RS = retreating side; AS = advancing side.

unpolished surface. Removal of the surface oxide by polishing explains the lower impedances related to the polished samples compared to the unpolished ones. The exposure of highly active substrates explains the increased electrochemical activity at the polished surface. This surface, after exposure to EXCO for EIS test, as presented in Fig. 12d, shows intragranular attack over larger areas at the surface in relation to the unpolished one. The most susceptible areas to corrosion attack are the grains with a high density of T1 phase which are rapidly attacked in the EXCO solution.

Due to the irregular characteristics of the welding joint, it was necessary to smoothen the surface prior to the exfoliation test; consequently, the electrochemical behavior of the welding zones was compared using polished surfaces. The EIS results showed that the highest impedances were related to the SZ, and the lowest, to the HAZ (LT), Fig. 13. The susceptibility to exfoliation increased in the following sequence, according to the EIS results: SZ < BM < HAZ (LT). These results are in accordance with the observations from the immersion test. Low impedances and only one-time constant are identified in the EIS diagrams for all the welding zones tested, showing the very high electrochemical activity of these zones when exposed to the EXCO solution. However, the indication of a "shoulder" at high frequencies of the results corresponding to the SZ suggests that part of the natural oxide layer remained at the surface of this zone. Surface observation by SEM after test confirmed intense corrosion attack at the HAZ (LT), Fig. 14a, confirming that this region is highly susceptible to exfoliation whereas the SZ showed intergranular attack when it was exposed to the electrolyte separately, Fig. 14b. The intergranular attack in the SZ must be related to the dissolution of T1 anodic phases dur-

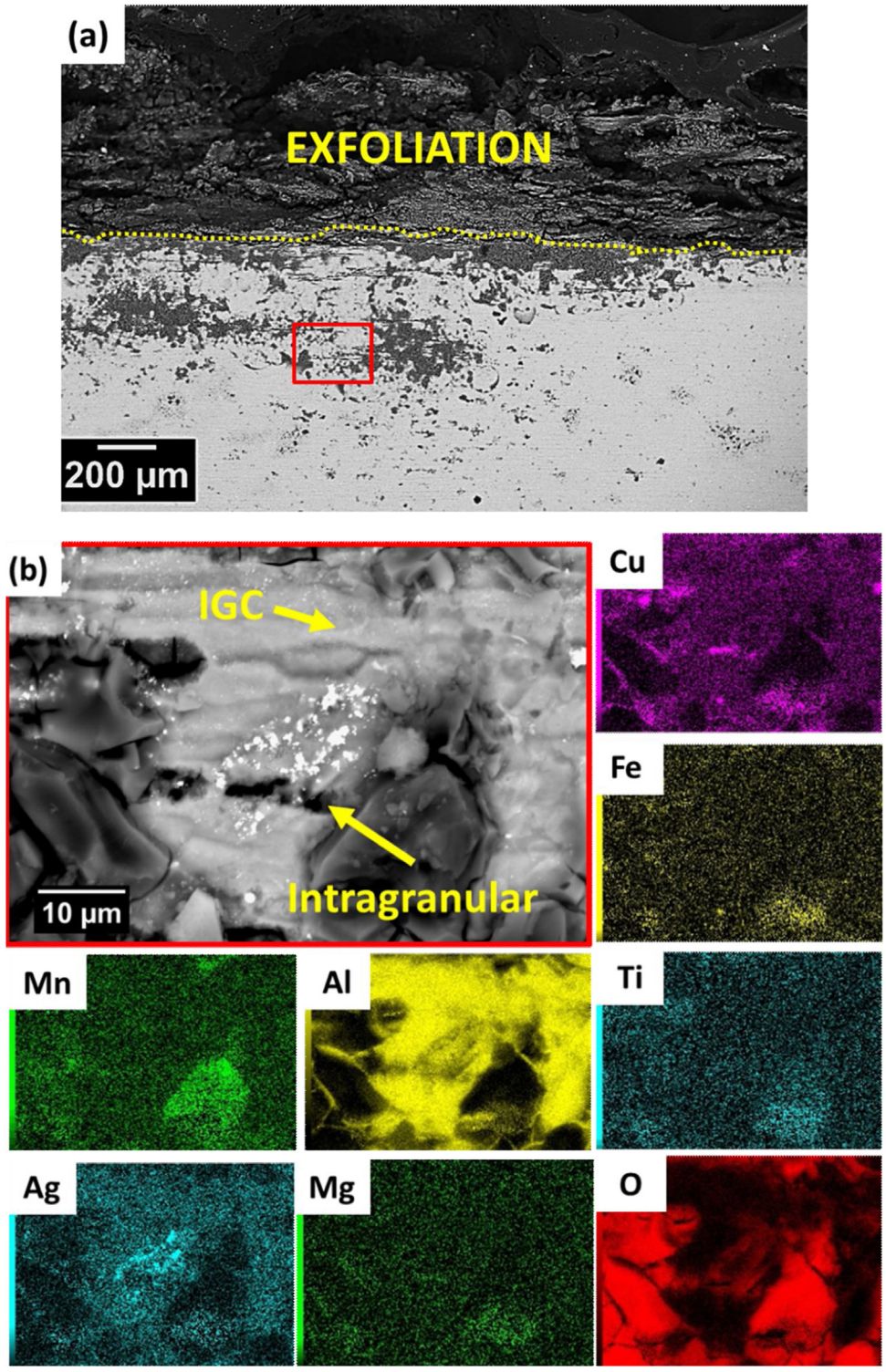

Fig. 9 – (a) SEM images of the HAZ (LT) in the AA2098-T351 alloy welded by FSW and exposed for 48 h to EXCO solution. (b) EDX maps from the squared region.

ing the welding process that favor intragranular attack, and the anodic nature of the GBs. It must be highlighted that intergranular attack appeared only in the welded joint, when the zones were isolated. Otherwise, when the welding zones were coupled, the welding joint was cathodically protected by the zones with high amounts of T1 phase, that is, HAZ (LT) and BM.

Table 1 summarizes the different types of corrosion propagation observed in the welding zones and their electrochemical behavior.

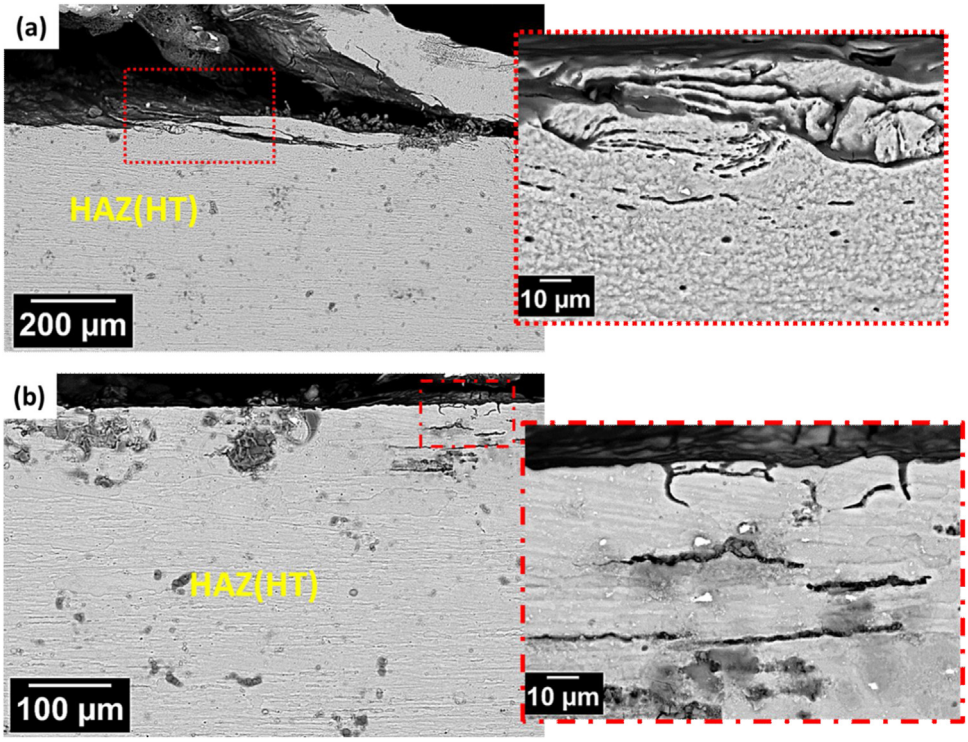

Fig. 10 – SEM images of the HAZ (HT) in the AA2098-T351 alloy welded by FSW and exposed for 48 h to EXCO solution. (a) retreating side; (b) advancing side.

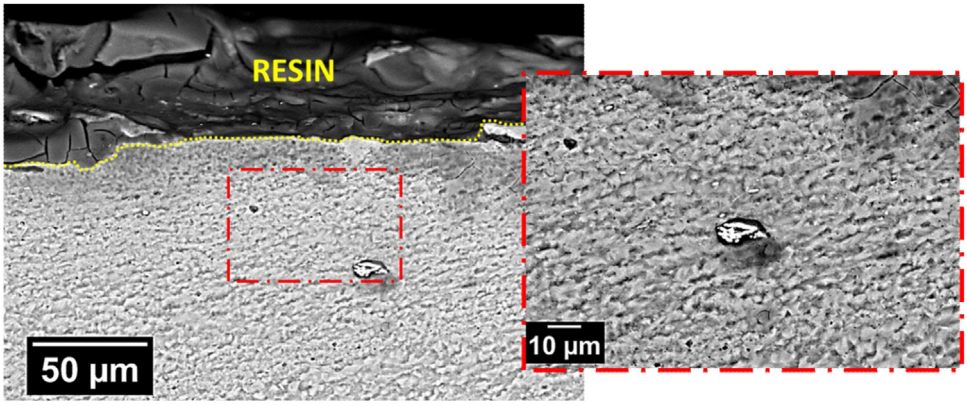

Fig. 11 – SEM images of the SZ in the AA2098-T351 alloy welded by FSW and exposed for 48 h to EXCO solution.

Table 1 – Corrosion features at different FSW zones exposed to EXCO solution.

Zone	Corrosion features		Electrochemical behavior
BM	Intragranular attack and exfoliation susceptibility		Anodic
HAZ (LT)	Intragranular attack, intergranular attack and exfoliation susceptibility		Anodic(high electrochemical activity)
HAZ (HT)	Intergranular attack		Cathodic
Weldingjoint			
ZTMA	Intergranular attack	(isolated)	Cathodic
SZ	Intergranular attack	(isolated)	Cathodic

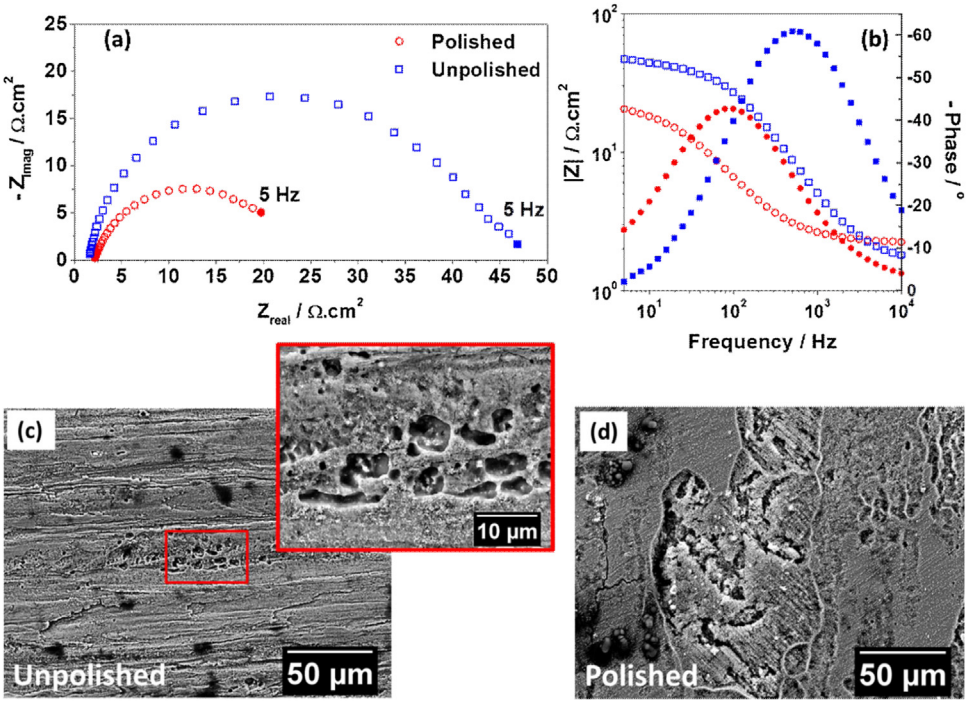

Fig. 12 – (a–b) EIS diagrams of the polished and as-received (unpolished) surfaces of the base metal (BM) of AA2098-T351 alloy after 1 h of immersion in EXCO solution. SEM images of the surface after exfoliation test in EXCO solution; (c) unpolished surface and (d) polished surface.

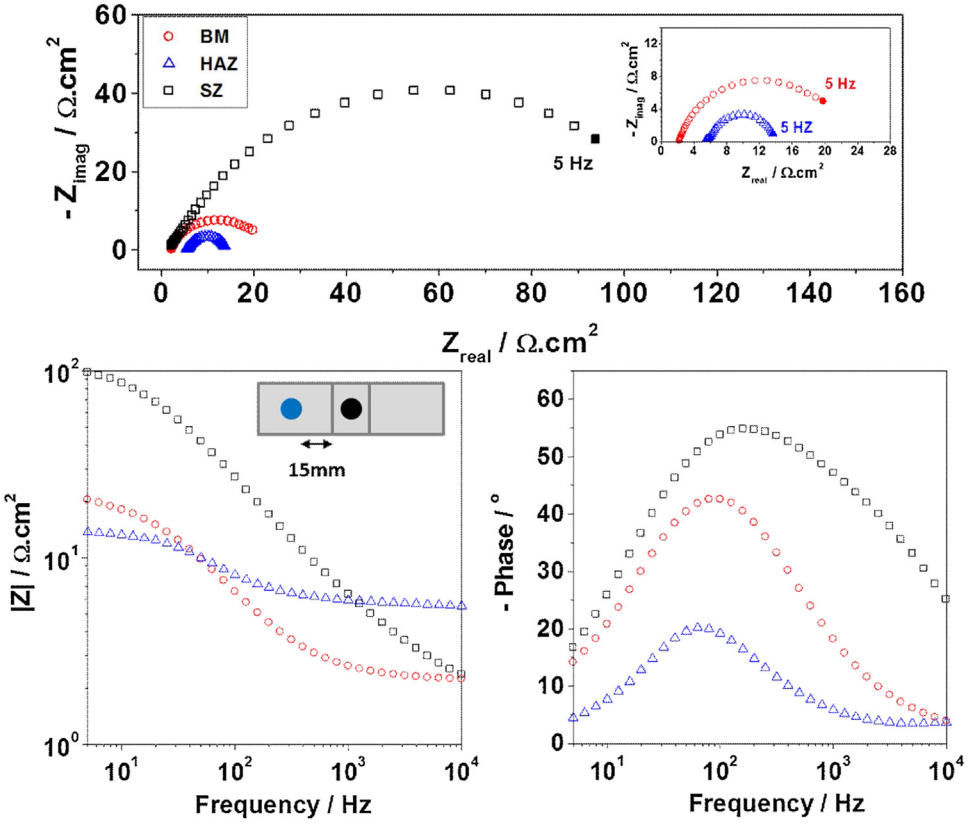

Fig. 13 – EIS diagrams of the different zones of the AA2098-T351 welded by FSW obtained from polished surfaces after 1 h immersion in EXCO solution.

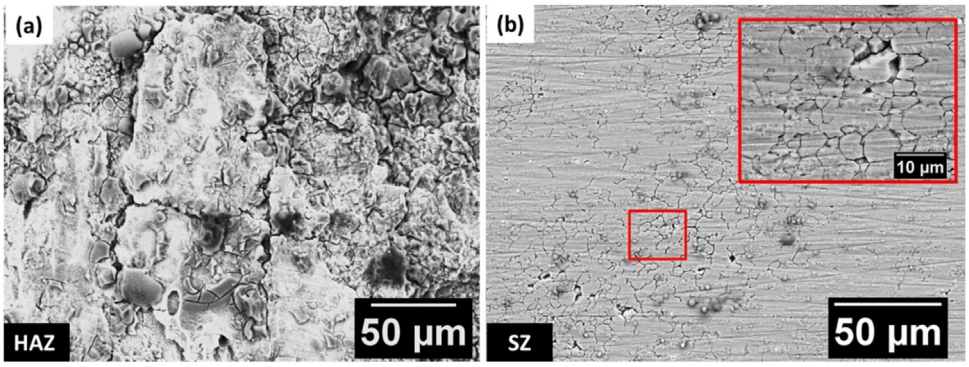

Fig. 14 – SEM images of the AA2098-T351 welded by FSW after EIS test in EXCO solution for 1 h; (a) heat affected zone (HAZ); (b) stir zone (SZ).

4. Conclusions

The susceptibility of the different zones of the AA2098-T351 processed by friction stir welding (FSW) to exfoliation was evaluated according to ASTM G34 standard practice and the results led to the following conclusions:

- The exfoliation mechanism of unwelded AA2098-T351 alloy was mainly associated with intragranular corrosion.
- The surface deformed layer present in the as-received (unpolished) alloy shows higher resistance to exfoliation compared to the bulk alloy (polished surface).
- FSW largely affected the resistance of the AA2098-T351 alloy to exfoliation and the various zones resulting from FSW showed different corrosion behaviors.
- Intergranular corrosion was observed in the stir zone when it was exposed to the electrolyte in isolation from the other zones.
- The base metal and the heat affected zone exposed to lower temperature (HAZ (LT)) were anodic to the other zones and provided cathodic protection to these zones when galvanically coupled.
- The high temperatures reached in the welding joint and the heat affected zone (HAZ (HT)) favored T1 phase dissolution and increased the resistance to exfoliation of these zones.
- The high susceptibility to exfoliation observed in the HAZ(LT) region showed that the precipitate free zone, coarse and small T1 phase, are critical factors for exfoliation propagation.

Acknowledgements

The authors acknowledge CAPES (Capes/Cofecub No 806-14) and FAPESP (2013/13235-6) for financial support for this work and to CAPES for the grants of M.X. Milagre (88882.333479/2019-01), C.S.C. Machado (88882.333459/2019-01) and FAPESP for the grants of U. Donatus (Proc.2017/03095-3) and R. Silva (Proc. 2018/06880-6). Acknowledgements are also due to Dr. Maysa Terada, Rafael Giorgão, Victor Ferrinho for the welding by FSW of the AA2098-T351 plate and Dr. Naga V. Mogili for the TEM images from Brazilian Nanotechnology National Laboratory (LNNano). Also, thanks are due to Dr. Antonello Astarita from University of Naples "Federico II", Italy Dept. of Chemical, Materials and Industrial Production Engineering for providing the alloy used in this study. Dr. Nadine Pebere, Dr. Emilie Lebon from the Institut National Polytechnique de Toulouse (INPT) and Sophie Regnier from the Institut Catholique d'Arts et Métiers (ICAM) for technical support in microhardness analysis. The authors are also grateful to Dr. Izabel Fernanda Machado from the University of São Paulo, Dept. of Mecatronic and Mechanical Systems for the support in the SEM analysis.

REFERENCES

[1] de Sousa Araujo JV, Donatus U, Queiroz FM, Terada M, Milagre MX, de Alencar MC, et al. On the severe localized corrosion susceptibility of the AA2198-T851 alloy. Corros Sci 2018;133:132–40.
[2] Donatus U, de Viveiros BVG, de Alencar MC, Ferreira RO, Milagre MX, Costa I. Correlation between corrosion resistance, anodic hydrogen evolution and microhardness in friction stir weldment of AA2198 alloy. Mater Charact 2018;144:99–112.
[3] Robinson MJ. Mathematical modelling of exfoliation corrosion in high strength aluminium alloys. Corros Sci 1982;22:775–90.
[4] Robinson MJ, Jackson NC. The influence of grain structure and intergranular corrosion rate on exfoliation and stress corrosion cracking of high strength AlCuMg alloys. Corros Sci 1999;41:1013–28.
[5] Kelly DJ, Robinson MJ. Influence of heat treatment and grain shape on exfoliation corrosion of Al-Li alloy 8090. Corros Sci 1993;49:787–95.
[6] Li C, Pan Q, Shi Y, Wang Y, Li B. Influence of aging temperature on corrosion behavior of Al-Zn-Mg-Sc-Zr alloy. Mater Des 2014;55:551–9.
[7] Marlaud T, Deschamps A, Bley F, Lefebvre W, Baroux B. Evolution of precipitate microstructures during the retrogression and re-ageing heat treatment of an Al-Zn-Mg-Cu alloy. Acta Mater 2010;58:4814–26.
[8] Donatus U, Terada M, Ospina CR, Queiroz FM, Fatima Santos Bugarin A, Costa I. On the AA2198-T851 alloy microstructure and its correlation with localized corrosion behaviour. Corros Sci 2018;131:300–9.
[9] Ma Y, Zhou X, Liao Y, Yi Y, Wu H, Wang Z, et al. Localised corrosion in AA 2099-T83 aluminium-lithium alloy: the role of grain orientation. Corros Sci 2015;107:41–8.

[10] Guérin M, Andrieu E, Odemer G, Alexis J, Blanc C. Effect of varying conditions of exposure to an aggressive medium on the corrosion behavior of the 2050 Al-Cu-Li alloy. Corros Sci 2014;85:455–70.
[11] Proton V, Alexis J, Andrieu E, Delfosse J, Lafont M-C, Blanc C. Characterisation and understanding of the corrosion behaviour of the nugget in a 2050 aluminium alloy Friction stir Welding joint. Corros Sci 2013;73:130–42.
[12] Li H, Tang Y, Zeng Z, Zheng F. Exfoliation corrosion of T6- and T8-aged AlxCuyLizalloy. Trans. Nonferrous Met. Soc. China (English Ed 2008;18:778–83.
[13] Yue X, Xiaojing W, Zhaotong Y, Jiaxue L. Corrosion properties of light-weight and high-strength 2195 Al-Li alloy. Chinese J Aeronaut 2011;24:681–6.
[14] Wenjie L, Qinglin P, Yunbin H, Yunchun L, Yingchun Z, Congge L. Effect of aging on the mechanical properties and corrosion susceptibility of an Al-Cu-Li-Zr alloy containing Sc. Rare Met Mater Eng 2008;27:146–52.
[15] Milagre MX, Mogili NV, Donatus U, Giorjão RAR, Terada M, Araujo JVS, et al. On the microstructure characterization of the AA2098-T351 alloy welded by FSW. Mater Charact 2018;140:233–46.
[16] Fonda RW, Bingert JF. Precipitation and grain refinement in a 2195 Al friction stir weld. Metall Mater Trans A Phys Metall Mater Sci 2006;37:3593–604.
[17] Shukla AK, Baeslack WA. Study of microstructural evolution in friction-stir welded thin-sheet Al-Cu-Li alloy using transmission-electron microscopy. Scr Mater 2007;56: 513–6.
[18] Shukla AK, Baeslack WA. Study of process/structure/property relationships in friction stir welded thin sheet Al-Cu-Li alloy. Sci Technol Weld Join 2009;14:376–87.
[19] Donatus U, Thompson GE, Zhou X, Wang J, Cassell A, Beamish K. Corrosion susceptibility of dissimilar friction stir welds of AA5083 and AA6082 alloys. Mater Charact 2015;107:85–97.
[20] de Abreu CP, Costa I, de Melo HG, Pébère N, Tribollet B, Vivier V. Multiscale electrochemical study of welded Al alloys joined by friction stir welding. J Electrochem Soc 2017;164:C735–46.
[21] Jariyaboon M, Davenport AJ, Ambat R, Connolly BJ, Williams SW, Price DA. The effect of welding parameters on the corrosion behaviour of friction stir welded AA2024-T351. Corros Sci 2007;49:877–909.
[22] Machado C, Donatus U, Xavier Milagre M, Mogili N, Giorjão R, Klumpp R, et al. Correlating the modes of corrosion with microstructure in friction stir welded AA2198-T8 alloy in aqueous hydrogen peroxide-chloride medium. Corrosion 2019;75:628–40.
[23] D'Urso G, Giardini C, Lorenzi S, Cabrini M, Pastore T. The effects of process parameters on mechanical properties and corrosion behavior in friction stir welding of aluminum alloys. Procedia Eng 2017;183:270–6.
[24] Donatus U, Berbel LO, Costa I. Qualitative use of potentiodynamic polarization and anodic hydrogen evolution in the assessment of corrosion susceptibility in AA2198-T851 Al – Cu – Li alloy. Mater Corros 2018:1–14.
[25] Milagre MX, Donatus U, Machado CSC, Araujo JVS, da Silva RMP, de Viveiros BVG, et al. Comparison of the corrosion resistance of an Al–Cu alloy and an Al–Cu–Li alloy. Corros Eng Sci Technol 2019;0:1–11.
[26] Chen MH, Hwang RY, Chou CP. Microstructure and corrosion properties of AA2091-T3 in weld heat a ff ected zone. Sci. Technol. Weld. Join 1999;4:21–7, http://dx.doi.org/10.1179/stw.1999.4.1.21.
[27] Keddam M, Kuntz C, Takenouti H, Schuster D, Zuili D. Exfoliation corrosion of aluminium alloys examined by electrode impedance. Electrochim Acta 1997;42:87–97.
[28] Zhang Z, Su JX, Shi YY, Cao FH, Zhang JQ. Exfoliation corrosion of Al-Li alloy 2090-T6 in EXCO solution: a study of electrochemical noise and electrochemical impedance spectroscopy. Mater Corros 2006;57:484–90.
[29] Song FX, Zhang XM, Liu SD, Tan Q, Li DF. Exfoliation corrosion behavior of 7050-T6 aluminum alloy treated with various quench transfer time. Trans Nonferrous Met Soc China (English Ed 2014;24:2258–65.
[30] Cabrini M, Lorenzi S, Bocchi S, Pastore T, D'Urso G, Giardini C. Evaluation of corrosion behavior of AA2024 T3 welded by means of FSW, EUROCORR 2017 - Annu. Congr. Eur. Fed. Corros. 20th int. Corros. Congr. Process saf. Congr. 2017; 2017. p. 1–15.
[31] Donatus U, Ferreira RO, Vardan Mogili NV, Gonçalves de Viveiros BV, Milagre MX, et al. Corrosion and anodizing behaviour of friction stir weldment of AA2198-T851 Al-Cu-Li alloy. Mater Chem Phys 2018;144:99–112.
[32] Liu B, Zhang X, Zhou X, Hashimoto T, Wang J. The corrosion behaviour of machined AA7150-T651 aluminium alloy. Corros Sci 2017;126:265–71.
[33] Luo C, Albu SP, Zhou X, Sun Z, Zhang X, Tang Z, et al. Continuous and discontinuous localized corrosion of a 2xxx aluminium-copper-lithium alloy in sodium chloride solution. J Alloys Compd 2016;658:61–70, http://dx.doi.org/10.1016/j.jallcom.2015.10.185.
[34] Kulinich SA, Akhtar AS, Wong PC, Wong KC, Mitchell KAR. Growth of permanganate conversion coating on 2024-Al alloy. Thin Solid Films 2007;515:8386–92.
[35] Nandan R, Debroy T, Bhadeshia HKDH. Recent advances in friction stir welding – process, weldment structure and properties. Prog Mater Sci 2008;53:980–1023.
[36] Zhang FD, Liu H, Subka C, Liu YX, Liu Z, Guo W, et al. Corrosion behaviour of laser-cleaned AA7024 aluminium alloy; 2017.
[37] Halder NC, Alonso JJ. Valence and core Electron spectra of Mg in MgO in evoporated thin films. J Phys Sci Sect A 1975;30:1485–90.
[38] CHEN PS, Bhat BN. Time-temperature-Precipitation behavior in AI-Li alloy 2195, tech. Rep; 2002 http://ntrs.nasa.gov/archive/nasa/casi.ntrs.nasa.gov/20020030744.pdf.
[39] Kumar KS, Brown SA, Pickens JR. Microstructural evolution during aging of an Al-Cu-Li-Ag-Mg-Zr alloy. Acta Mater 1996;44:1899–915.
[40] Meininger JM, Dickerson SL, Gibeling JC, Meiningers M, Son LD, Ling JCG, et al. Observations of tension/compression asymmetry in the cyclic deformation of aluminum alloy 7075. Fatigue Fract Eng Mater Struct 1996;19:85–97.
[41] Guérin M, Alexis J, Andrieu E, Laffont L, Lefebvre W, Odemer G, et al. Identification of the metallurgical parameters explaining the corrosion susceptibility in a 2050 aluminium alloy. Corros Sci 2016;102:291–300.
[42] Donatus U, ThompsoN GE, Omotoyinbo JA, Alaneme KK, Aribo S, Agbabiaka OG. Corrosion pathways in aluminium alloys. Trans Nonferrous Met Soc China 2017;27:55–62.
[43] Zhang X, Zhou X, Hashimoto T, Lindsay J, Ciuca O, Luo C, et al. The influence of grain structure on the corrosion behaviour of 2A97-T3 Al-Cu-Li alloy. Corros Sci 2017;116:14–21.
[44] Grosskreutz JG. The mechanisms of metal fatigue (II). Phys Status Solidi 1971;47:359–96.
[45] Al-Rubaie KS, Del Grande MA, Travessa DN, Cardoso KR. Effect of pre-strain on the fatigue life of 7050-T7451 aluminium alloy. Mater Sci Eng A 2004;464:141–50.
[46] Hughes AE, Boag A, Glenn AM, McCulloch D, Muster TH, Ryan C, et al. Corrosion of AA2024-T3 part II: co-operative corrosion. Corros Sci 2011;53:27–39.
[47] Hughes AE, Birbilis N, Mol JMC, Garcia SJ, Zhou X, Thompson GE. High strength Al-Alloys: microstructure, corrosion and

principles of protection, in: recent trends process. Degrad Alum Alloy InTech 2011:223–62.
[48] Murayama M, Hono K. Role of Ag and Mg on precipitation of T1phase in an Al-Cu-Li-Mg-Ag alloy. Scr Mater 2001;44:701–6.
[49] Bocchi S, Cabrini M, D'Urso G, Giardini C, Lorenzi S, Pastore T. The influence of process parameters on mechanical properties and corrosion behavior of friction stir welded aluminum joints. J Manuf Process 2018;35:1–15.